MEMS Lorentz Force Magnetometers

Agustín Leobardo Herrera-May, Francisco López-Huerta and Luz Antonio Aguilera-Cortés

Abstract Lorentz force magnetometers based on microelectromechanical systems (MEMS) have several advantages such as small size, low power consumption, high sensitivity, wide dynamic range, high resolution, and low cost batch fabrication. These magnetometers have potential applications in biomedicine, navigation systems, telecommunications, automotive industry, space satellites, and non-destructive testing. This chapter includes the development of MEMS magnetometers composed by resonant structures that use the Lorentz force and different signal processing techniques. In addition, it presents the operation principle, sensing techniques, fabrication processes, applications, and challenges of MEMS magnetometers. Future applications will consider the integration of magnetometers with different devices (e.g., accelerometers, gyroscopes, energy harvesting and temperature sensors) on a single chip.

1 Introduction

The miniaturization has enabled the fabrication of different elements on the same chip: sensors, actuators, electronics, communication, computation, signal processing and control [1]. This chip can be developed using the batch production of micro-

A.L. Herrera-May (✉)
Micro and Nanotechnology Research Center, Universidad Veracruzana, Calzada Ruiz Cortines 455, 94294 Boca Del Rio, VER, Mexico
e-mail: leherrera@uv.mx

F. López-Huerta
Engineering Faculty, Universidad Veracruzana, Calzada Ruiz Cortines 455, 94294 Boca Del Rio, VER, Mexico
e-mail: frlopez@uv.mx

L.A. Aguilera-Cortés
Depto. Ingeniería Mecánica, DICIS, Universidad de Guanajuato, Carretera Salamanca-Valle de Santiago 3.5 + 1.8 Km, 36885 Salamanca GTO, Mexico
e-mail: aguilera@ugto.mx

A. Grosz et al. (eds.), *High Sensitivity Magnetometers*, Smart Sensors, Measurement and Instrumentation 19, DOI 10.1007/978-3-319-34070-8_9

fabrication processes, which can reduce its cost. The miniaturization is key to produce chips with important characteristics such as multiple functions, small size, low-energy consumption, and high performance. For instance, the recent computing systems are much more powerful and faster than those available 20 years ago. They include more features, are significantly cheaper, and have far less power consumption. Miniaturization has achieved faster devices with considerable cost/performance advantages and the integration of mechanical and fluidic parts with electronics. Thus, these devices can increase their functionality, resolution and sensibility.

1.1 MEMS

Microelectromechanical systems (MEMS) have allowed the development of devices composed by electrical and mechanical components with size in the micrometer-scale, which can include signal acquisition, signal processing, actuation, and control [2]. These devices offer several advantages such as small size, reduced power consumption, high sensitivity, and low cost batch fabrication. Recently, several MEMS devices have been fabricated such as micromirrors, accelerometers, gyroscopes, magnetometers, pressure sensors, micropumps, and microgrippers [3–10]. These devices could be employed in biomedical and chemical analyses, automobile and military industries, telecommunications, consumer electronic, and navigation. Figure 1 depicts SEM image of two MEMS magnetometers designed by researchers from Micro and Nanotechnology Research Center (MICRONA-UV) into collaboration with Microelectronics Institute of Barcelona (IMB-CNM, CSIC).

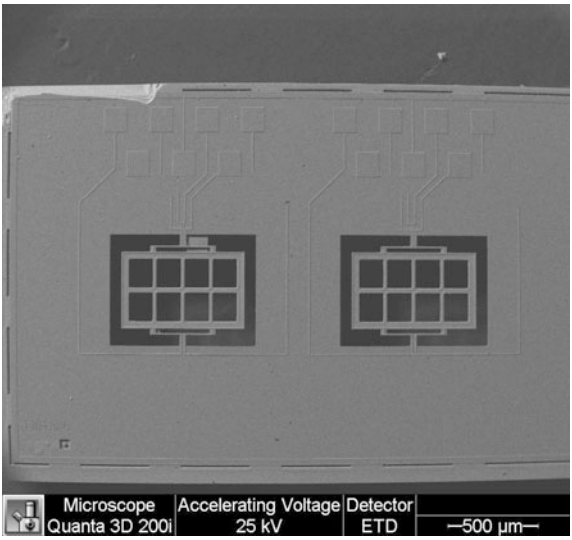

Fig. 1 SEM image of two magnetometers based on resonant silicon structures and piezoresistive sensing. These magnetometers are designed by researchers from MICRONA-UV and IMB-CNM (CSIC)

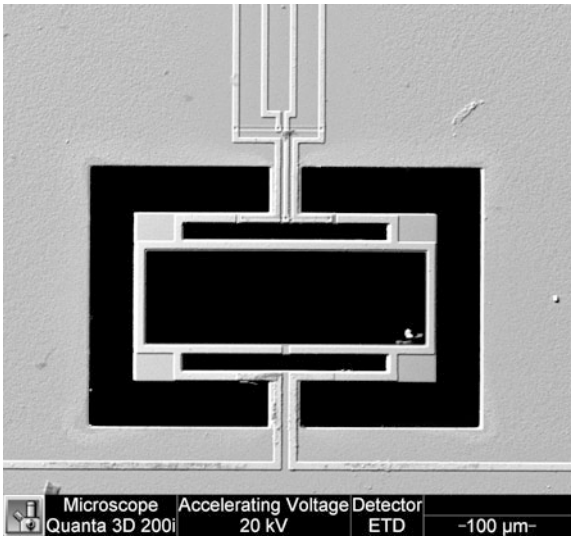

Fig. 2 SEM image of a MEMS magnetometer with piezoresistive sensing, which is developed by researchers from MICRONA-UV and IMB-CNM (CSIC)

The classification of MEMS considers three groups: micromechanical structures, actuators, and sensors [2]. Micromechanical structures can include beams, plates, and microchannels. Actuators convert magnetic or electrical input signals to motions (e.g., resonant structures, micropumps, microgrippers, and microswitches). Sensors detect chemical and physical signals, which are transformed to electrical signals. Figure 2 depicts SEM image of a magnetometer with piezoresistive sensing, which has a resonant silicon structure and a Wheatstone bridge with four p-type piezoresistors. This magnetometer is fabricated by researchers from MICRONA-UV and IMB-CNM (CSIC).

Fabrication of MEMS devices with their microelectronics on a single chip allows integrated devices. They combine microelectromechanical structures, sensing elements, and signal conditioning. These devices will permit new applications, incorporating the advantages of MEMS and microelectronics. The integration of MEMS devices with signal conditioning systems on a single chip can active the design of different devices to monitor several chemical and physical variables. For example, multiaxis MEMS accelerometers and gyroscopes may be applied in smartphones to control the screen orientation.

1.2 Fabrication Processes

MEMS devices can be fabricated using surface and bulk micromachining techniques. These techniques take advantage of both mechanical and electrical properties of the silicon. Silicon mechanical properties have a higher strength than the steel and a minimum mechanical hysteresis. In addition, silicon electrical properties have allowed it to be the most common material of integrated circuits.

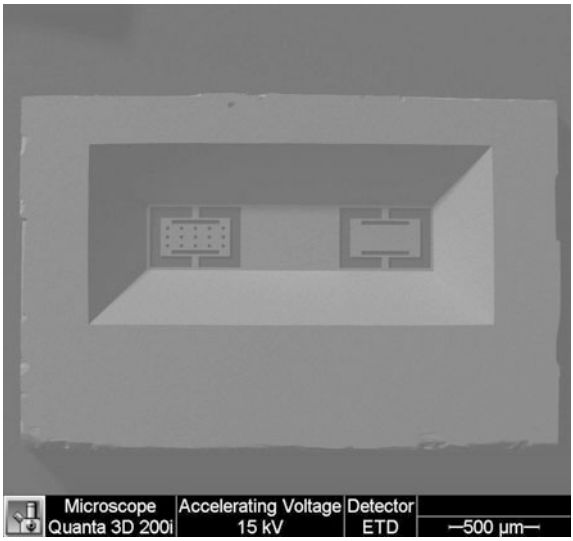

Fig. 3 SEM image of two resonant silicon structures (*backside view*) that are fabricated using bulk micromachining. These magnetometers are designed by researchers from MICRONA-UV and IMB-CNM (CSIC)

Bulk micromachining selectively etches a silicon substrate to fabricate three-dimensional microstructures. In this micromachining process, a great amount of material is removed from silicon wafer to develop beams, membranes, holes, microchannels, and other structures types (see Fig. 3). Etching techniques, during the MEMS fabrication, eliminate materials in desired areas through physical or chemical processes, which define the geometry shape of the MEMS components. Usually chemical etching is referred as wet etching and the physical etching is named as dry or plasma etching. Chemical etching considers solutions with diluted chemicals to dissolve substrates. For example, potassium peroxide (KOH) is employed to etch silicon dioxide (SiO_2), silicon nitride (Si_3N_4), and polycrystalline silicon. Plasma etching generates a stream of positive-charge-carrying ions of a substance with a large number of electrons, which is diluted with inert carrier gas such as argon [11]. It is achieved using a high-voltage electric charge or radiofrequency (RF) sources. This micromachining technology is based on sculpting features in the bulk of the silicon substrate by orientation-independent (isotropic) or orientation-dependent (anisotropic) wet or dry etchants. Wet etching provides higher degree of selectivity than the dry etching [12]. For these etching processes, the etch-stop is related with the crystal orientation or dopant concentration of silicon wafer as well as etchant protection masks, which are not selective to the used etching type. In this technology is key the etching type employed to fabricate the microstructures.

Generally, bulk micromachining take advantages of materials such as silicon, silicon carbide (SiC), gallium arsenide (GaAs), indium phosphide (InP), germanium (Ge), and glass. An etching protection mask covers a part of the material substrate, which is used to protect it of chemical etchants. However, the other part of the silicon substrate without etching protection mask is dissolved by the etchants. Moreover, the chemical etching may undercut a silicon part located under the protective mask. Etching process of the silicon substrate can be isotropic or

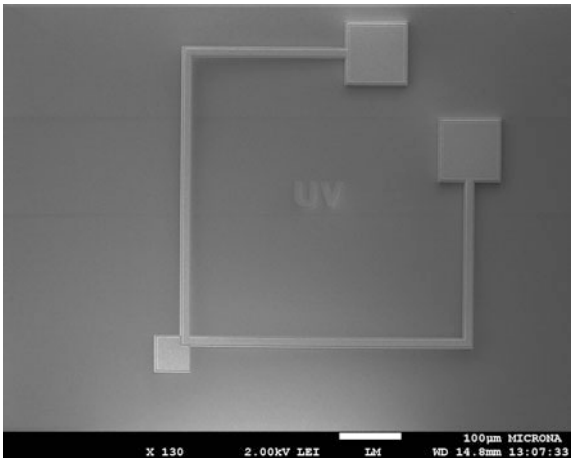

Fig. 4 SEM image of a magnetometer composed by a polysilicon resonator, a micromirror, and an aluminum loop. It is designed by researchers from MICRONA-UV and fabricated using the Sandia Ultra-planar Multi-level MEMS technology (SUMMiT V) process

anisotropic. Isotropic etching attacks in all directions the silicon substrate, which is called orientation-independent etching. This etching type depends of the temperature and has difficult to control the lateral etching of the substrate. On the other hand, anisotropic etching achieves defined well geometry shapes of microstructures due to crystallographic planes of the substrate.

Surface micromachining is based on patterning layers deposited on the silicon surface or any other substrate. It lets the integration of MEMS devices with microelectronics on the same substrate. The thickness of the structural layer is determined by the thickness of the deposited layer. This micromachining process can deposit layers on silicon substrate using the low-pressure chemical vapor deposition (LPCVD) technique. Polysilicon is the most common structural material for surface micromachining. Sacrificial layers (e.g., SiO_2 or phosphorus silicon glass) define the space between the structural layers and substrate, which are removed with wet etching. Thus, the structural layers are suspended (see Fig. 4). In the wet etching the surface tension force may pull the structural layers, causing permanent stiction. Structural layers can be polysilicon, Si_3N_4, polymide, titanium, and tungsten, which can have thickness from 2 to 5 μm. These layers require high temperature treatment to relief their internal stresses generated during the surface micromachining. This fabrication process is much more complex than bulk micromachining.

1.3 Sensing Techniques

MEMS devices can detect different physical, biological or chemical phenomena through piezoresistive, capacitive, or piezoelectric sensing techniques. The selection suitable of a sensing technique for monitoring chemical or physical signal depends of signal dynamic range, environmental parameters, packaging, and required accuracy. Environmental parameters include operating pressure and

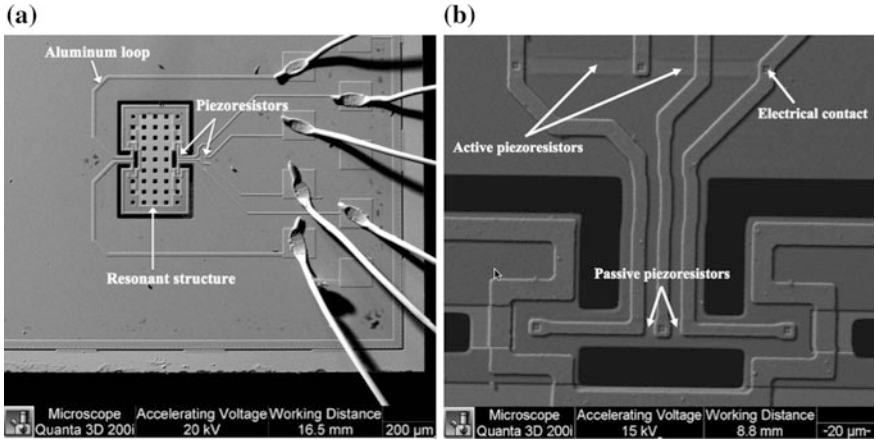

Fig. 5 SEM image of a MEMS magnetometer with piezoresistive sensing. **a** Resonant silicon structure and aluminum loop; **b** four piezoresistors of a Wheatstone bridge [13]. Reprinted with permission from Herrera-May et al., Microelectron. Eng., 142, 12–21, 2015. Copyright © 2015, Elsevier B.V

temperature, moisture, and chemical exposure. In addition, other factors can affect the choice of the sensing technique such as signal processing, data display, device impedance, supply voltage, operating life, frequency response, and calibration.

Piezoresistive sensing is based on the resistance shift of a material when it is mechanically stressed. It can use a Wheatstone bridge of four piezoresistors to convert the variation of piezoresistors resistance to an output voltage shift, as shown in Fig. 5a, b. This sensing technique has a high dependence with respect to piezoresistor doping level and type, as well as operating temperature change. Piezoresistive sensing generates voltage offset in the electrical response of the MEMS device. Other variable resistive elements can be included to adjust the zero-offset level and calibrate the sensitivity, as well as provide temperature compensation. In addition, a temperature dependence of full-scale span (i.e., difference between full-scale output and offset) could be controlled applying suitable doping levels.

Capacitive sensing uses the capacitance variation between electrodes with plates or beams shapes. They provide fixed and moving electrodes that are relatively straightforward to fabricate. This technique must consider interdigitated capacitors and effects of the fringing fields. It is less noisy that piezoresistive sensing but its values of capacitance are extremely small. It can use charge amplifiers, charge balance technique, ac bridge impedance measurements, and several oscillator configurations.

Optical sensing relies on modulating the properties of an optical frequency electromagnetic wave. A MEMS device can module a property of the electromagnetic wave such as intensity, phase, wavelength, frequency, spatial position, and polarization.

Piezoelectric sensing employs piezoelectric materials to generate an electrical signal when they are mechanically deformed. MEMS devices with piezoelectric

elements can produce an output voltage when they are strained. Piezoelectric material as lead zirconate titanate (PZT) is a common material for MEMS devices. Piezoelectric sensing is inexpensive and it does not require a supply voltage. However, piezoelectric materials can lose their piezoelectric properties with temperatures close to their Curie points. In addition, piezoelectric coefficients of these materials depend the temperature change.

1.4 Packaging Process

Packaging process is key for establishing the reliability of MEMS devices. The package offers protection from environmental parameters such as moisture, liquid or gaseous chemicals. MEMS devices can use ball-grid array (BGA) and land-grid array (LGA) packages. Furthermore, surface-mount technology (SMT) can provide wafer-level packages (WLPs), stacked die, wafer-level chip-scale packages (WLCSPs), and 3-D packaging. The cost of a MEMS device can increase about 35–60 % due to the packaging, assembly, test, and calibration steps, as well as the application-specific integrated circuit (ASIC) [14]. After of fabrication process, the MEMS devices are separated into individual die from the wafer by sawing or scribe-and-break techniques. These dice are placed in carriers with automatic pick-and-place machines to move the dice from the carrier to the package, where device die is bonded to a package, as shown in Fig. 6. Next, wire bonds connect the electrical contacts (pads) of the die surface with those of the package, as shown in Fig. 7. It allows the electrical connections between the device and external components.

The design of a MEMS device packaging must take into account the device-specific function and the sensing technique, as well as the thermal stress produced during the packaging process. This thermal stress alters the device sensitivity and resolution. The device packaging can be affected by the characteristic

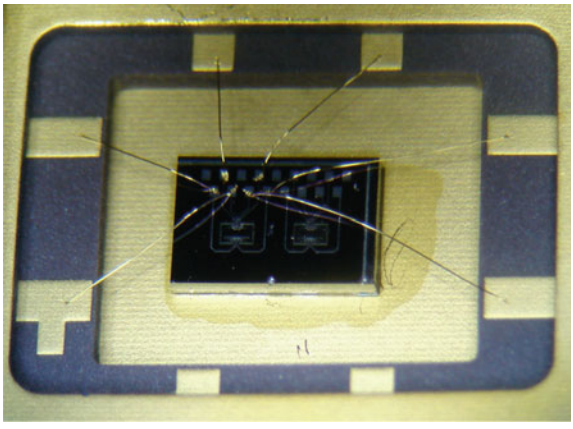

Fig. 6 Microphotography of a packaged MEMS magnetometer, which is fabricated by researchers from MICRONA-UV and IMB-CNM (CSIC)

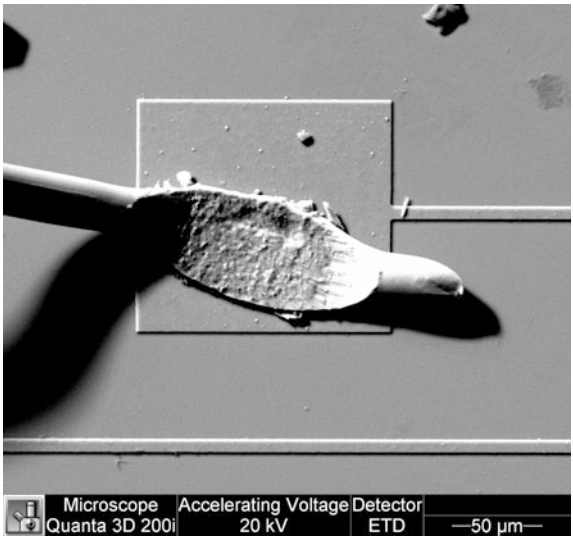

Fig. 7 SEM image of an electrical contact of a gold wire with a MEMS device pad. It is developed by researchers from MICRONA-UV and IMB-CNM (CSIC)

following: wafer thickness and wafer stack, dimensions, integration level, stress sensitivity, environmental sensitivity, heat generation, heat sensitivity, and light sensitivity [10].

1.5 Reliability

MEMS devices require reliability tests to verify their performance under different environmental and operating conditions. These tests can involve operational life, temperature cycling, mechanical shock, humidity variations, high temperature, and vibrations. The lifetime reliability of MEMS devices can be obtained through accelerated life and mechanical integrity testing. For these devices, several failure mechanisms occur during the fabrication, packaging, and signal conditioning processes.

2 Lorentz Force Magnetometers

MEMS-based Lorentz force magnetometers are an alternative for monitoring magnetic field with important advantages such as small size, low power consumption, high sensitivity, good resolution, wide dynamic range, and low cost by using batch fabrication. These magnetometers are small and lightweight compared

to SQUIDs devices, search coil sensors, and fiber optic sensors. They could be commercially competitive with respect to anisotropic magnetoresistive (AMR) and giant magnetoresistive (GMR) sensors, and Hall-effect devices. However, MEMS magnetometers need more reliability studies to ensure a safe performance under different environmental conditions.

2.1 Operation Principle

MEMS Lorentz force magnetometers can operate with silicon-based structures, which interact with an external magnetic field and an electrical current to generate a Lorentz force on the structures. This force is perpendicular to the direction of both magnetic field and electrical current. It causes a deformation of the magnetometer structure that can be measured by using a capacitive, piezoresistive, or optical sensing technique. In order to increase the sensitivity of the magnetometer is recommended to operate its structure at resonance. For this, electrical current is applied with a frequency equal to the resonant frequency of the magnetometer structure. This structure at resonance can increase the magnetometer sensitivity by a parameter equal to its quality factor. Thus, the magnetic field signal can be converted in electrical or optical signal. Figure 8 shows the operation principle of a Lorentz force magnetometer, in which the Lorentz force is obtained as:

$$F_L = I_e B_x L_y \tag{1}$$

with

$$I_e = \sqrt{2} I_{RMS} \sin(\omega t) \tag{2}$$

where L_y is the width of the perforated plate, t is the time, and I_{RMS} and ω are the root-mean-square (RMS) and circular frequency of the sinusoidal electrical current (I_e), respectively.

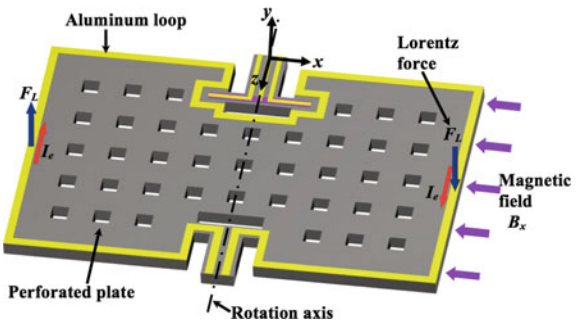

Fig. 8 Schematic view of the operation principle of a MEMS-based Lorentz force magnetometer [13]. Reprinted with permission from Herrera-May et al., Microelectron. Eng., 142, 12–21, 2015. Copyright © 2015, Elsevier B.V

Lorentz force causes a deflection of the magnetometer structure and longitudinal strain (ε_l) of two active piezoresistors (tensile in one, compressive in the other). This strain increases when the magnetometer structure oscillates at resonance. This strain changes the initial resistance (R_i) of each active piezoresistor:

$$\Delta R_i = \pi_l E \varepsilon_l R_i \tag{3}$$

where ΔR_i is the resistance variation of the piezoresistor, E is the Young's modulus of the piezoresistor material and π_l is the longitudinal piezoresistive coefficient.

The resistance variation of the two piezoresistors alters the output voltage (V_{out}) of the Wheatstone bridge. It can be calculated as

$$V_{out} = \frac{1}{2} \pi_l E \varepsilon_l R_i V_{in} \tag{4}$$

where V_{in} is the bias voltage of the Wheatstone bridge.

The magnetometer sensitivity (S) can be determined as the ratio of the output voltage shift (ΔV_{out}) to the range of the magnetic field (ΔB_x) applied in parallel direction to the magnetometer length:

$$S = \frac{\Delta V_{out}}{\Delta B_x} \tag{5}$$

2.2 Materials

The performance of MEMS magnetometers strongly depends of the functional and structural materials. These magnetometers can have single-crystal silicon (SCS) or polysilicon as materials due to their important electrical and mechanical properties. In addition, different thin films materials can be used in MEMS magnetometers. Although, they have properties related with their fabrication process and post-process such as deposition conditions, annealing, deposition apparatus, and film thickness.

Accurate material properties of MEMS magnetometers should be known to predict their performance. Material properties can be measured using microfabricated test structures on the same wafer. For instance, test structures are used to detect Young's modulus, Poisson ratio, fracture stress, fracture toughness, fatigue, thermal conductivity, and specific heat measurement [15].

2.3 Simulation and Design Tools

Design stage of MEMS devices incorporate computer-aided simulation tools with the following advantages:

1. Prediction of devices performance related with different operation conditions, materials, and geometrical dimensions.
2. Syntheses to define optimal operation conditions, dimensions and materials of the devices.
3. Possibility to solve complex partial differential equations related with the devices performance.
4. Feasibility to develop robust and rapid design software tools that help designers to reduce the design time of devices.

Simulations tools are useful to predict the optimal design of MEMS magnetometers. It could help to designers to minimize the cost, size, weight, and losses, as well as maximize the sensibility and resolution of devices.

2.4 Damping Mechanisms

The performance of MEMS devices based on resonant structures is affected by damping mechanisms. The three main damping sources regard the energy lost to surrounding fluid, energy internally dissipated in the material, and vibrating energy dissipated through the support type of the devices. These damping mechanisms modify the quality factor (Q) of resonant structures, which is defined as the ratio of the total energy stored in the device structure to the energy lost per cycle.

Quality factor (Q_f) related with the energy lost to surrounding fluid is affected by the fluid type, structure size and vibration mode, and fluid pressure. It significantly increases when the fluid pressure decreases to values close to vacuum pressure [16, 17].

Thermoelastic damping implicates internal energy dissipation in the structure material. This damping involves a quality factor (Q_i) that depends of the oscillating temperature gradient of resonant structure and the materials thermal properties. It has a maximum magnitude for pressures near to vacuum [18].

Support damping can be defined as the vibration energy dissipated by its transmission through the structure supports. The quality factor (Q_s) associated with the support damping depends of support type of the resonant structure, vibration mode, and dimensions of the structure [19].

Total quality factor (Q_T) of a resonant structure is approximated as:

$$\frac{1}{Q_T} = \frac{1}{Q_f} + \frac{1}{Q_i} + \frac{1}{Q_s} \tag{6}$$

2.5 Classifications

MEMS magnetometers can be classified considering their sensing techniques such as capacitive, piezoresistive or optical. These techniques can convert a magnetic signal into an electrical or optical signal. They use signal conditioning systems integrated by electronic or optics components. Figure 9a, b depicts a schematic view of a Lorentz force based magnetometer with piezoresistive sensing [3]. Magnetometers with piezoresistive sensing have a simple signal processing and low cost fabrication. However, they require compensation circuits to reduce the effect of the temperature shifts on the magnetometers performance.

Generally, capacitive sensing is employed in magnetometers fabricated with surface micromachining, which allows the reduction of size and cost of magnetometers. This technique is impacted by parasitic capacitances, which are minimized through monolithic integration of magnetometers with the signal conditioning systems. Figure 10a, b shows a schematic view of a Lorentz force based magnetometer with capacitive sensing [3]. It incorporates a resonant plate with two torsional beams, an aluminum loop, and electrodes.

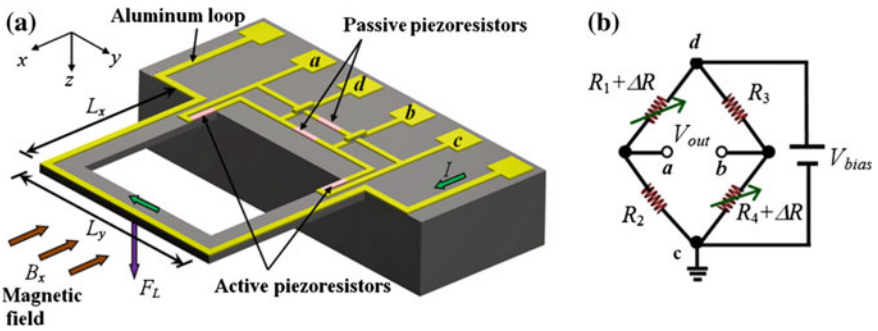

Fig. 9 **a** Schematic view of a Lorentz force based magnetometer with piezoresistive readout and **b** its Wheatstone bridge of four piezoresistors [3]. Reprinted with permission from Herrera-May et al., Sensors, 9, 7785–7813, 2009. Copyright © 2009, MDPI AG

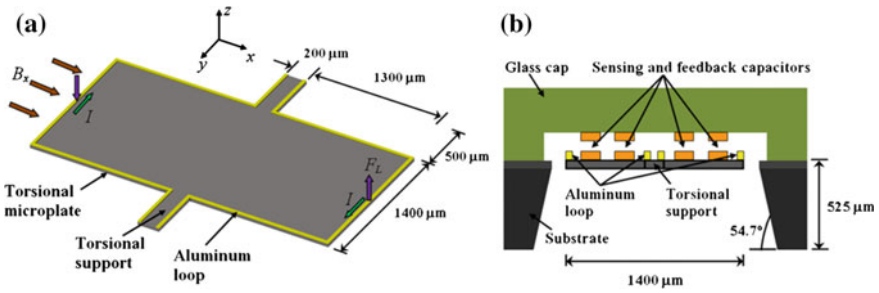

Fig. 10 **a** Schematic view of a Lorentz force based magnetometer composed by a resonant plate and **b** its capacitive readout system [3]. Reprinted with permission from Herrera-May et al., Sensors, 9, 7785–7813, 2009. Copyright © 2009, MDPI AG

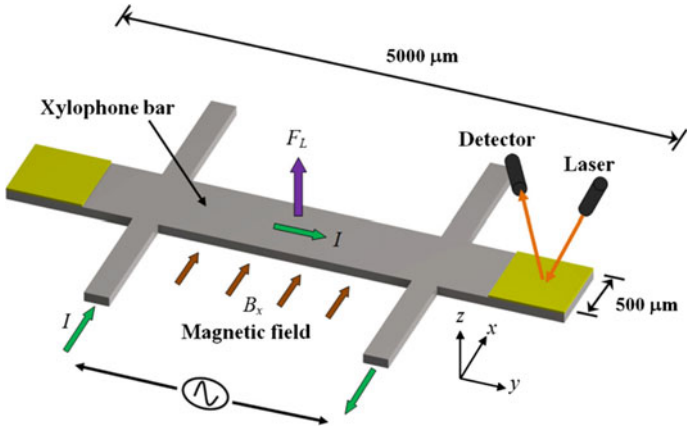

Fig. 11 Schematic view of a Lorentz force based magnetometer with resonant structure and optical sensing [3]. Reprinted with permission from Herrera-May et al., Sensors, 9, 7785–7813, 2009. Copyright © 2009, MDPI AG

Optical sensing allows a decrease of the electronic components and weight of the magnetometers. It has immunity to electromagnetic interference (EMI). A Lorentz force based magnetometer with a resonant structure and an optical readout system can measure external magnetic field through the displacements of its resonator, as shown in Fig. 11.

3 Transduction Techniques

This section presents the description of several MEMS magnetometers based on Lorentz force with different sensing techniques. It involves the main performance characteristics of the magnetometers.

3.1 Piezoresistive Sensing

Herrera-May et al. [20] designed a magnetometer formed by a silicon plate (400 × 150 × 15 μm), an aluminum loop, and a Wheatstone bridge with four p-type piezoresistors (see Fig. 12). It has a simple resonant structure fabricated using bulk micromachining. This plate operates at resonance (136.52 kHz) with a bending vibration mode, which rises its sensitivity to 403 mV T^{-1}. This magnetometer has a high quality factor of 842 at atmospheric pressure and a low power consumption about 10 mW. It uses a piezoresistive sensing, which has a non-linear electrical response with a high offset (close to 4 mV) under an external magnetic field. It registered a theoretical noise voltage of 57.48 nV $Hz^{-1/2}$, including the thermal noise, 1/*f* noise, and amplifier noise.

Later, Herrera-May et al. [21] developed a magnetometer based on a resonant structure composed by a silicon-beams rectangular loop (700 × 400 × 5 μm), an aluminum coil, and a piezoresistive sensing technique (see Fig. 13). It operates in bending vibration mode with a resonant frequency of 22.99 kHz at atmospheric pressure. Furthermore, it has a simple structure fabricated using bulk micromachining. This magnetometer has several advantages, including linear response, a

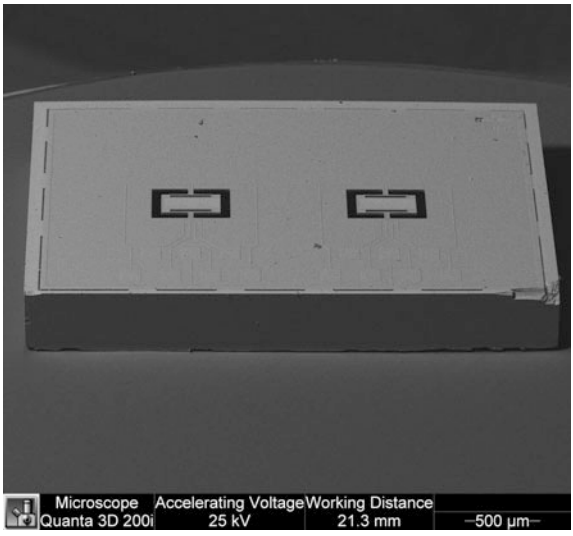

Fig. 12 SEM image of two MEMS magnetometers developed by Herrera-May et al. [20]. It was designed by researchers from MICRONA-UV and IMB-CNM (CSIC)

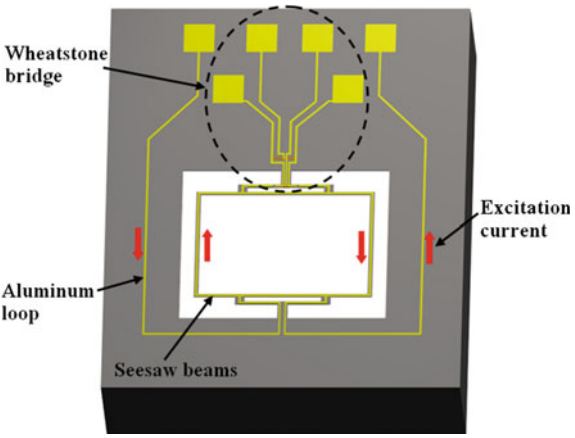

Fig. 13 3D schematic view of a magnetometer design developed by Herrera-May et al. [21]. Reprinted with permission from Herrera-May et al., Sens. Actuators A, 165, 399–409, (2011). Copyright © 2011, Elsevier B.V

quality factor of 96.6, a power consumption close to 16 mV, and a sensitivity of 1.94 V T^{-1}. In addition, it registered a theoretical noise voltage of 83.60 nV $Hz^{-1/2}$. Also, its electrical response registered a high offset due to residual stresses generated during the fabrication process and the Joule effect on the structure caused by the excitation electrical current.

Dominguez-Nicolas et al. [22] fabricated a magnetometer with a signal conditioning system and virtual instrumentation for industrial applications. This signal conditioning system is implemented on a printed circuit board (PCB). The magnetometer has a resonant silicon structure (700 × 600 × 5 μm) integrated by transversal and longitudinal beams, an aluminum loop, and a Wheatstone bridge with four p-type piezoresistors. This structure works in its first bending resonant frequency (14.38 kHz) and has a sensitivity of 4 V T^{-1}. With the signal conditioning system, the output signal of the magnetometer is digitally processed and converted in an industrial standard 4–20 mA output. This output signal has a linear behavior for small magnetic field.

3.2 Capacitive Sensing

Brugger and Paul [23] reported a magnetometer composed by a pair of planar coils and a silicon resonant structure (25 μm thick) with an amorphous magnetic concentrator, which is suspended by four straight flexural springs. It is fabricated with bulk micromachining using a silicon-on-insulator (SOI) substrate. The magnetometer has an electrostatically driven micromachined resonator, which uses capacitive detection. The stiffness and fundamental resonant frequency of the magnetometer is altered by an external magnetic field parallel to the magnetic concentrator. Thus, this resonant frequency shift is related with the applied magnetic field. For a coil current of 80 mA and a pressure of 10^{-5} mbar, the magnetometer reaches a sensitivity of 1.0 MHz T^{-1}, a resolution of 400 nT, and a high

quality factor close to 2400. This magnetometer does not need complex feedback and modulation electronics. However, it requires a post-fabrication process to collocate the magnetic concentrator on the resonant structure as well as a vacuum packaging. Large external mechanical vibrations can affect the magnetometer performance.

Li et al. [24] developed a magnetometer with a resonant polysilicon structure (15 μm thick) for monitoring both out-of-plane and in-plane magnetic field components. It requires capacitive sensing to detect the in-plane and out-of-plane motions of the resonant structure. The magnetometer is fabricated through standard surface micromachining process. It has low power consumption (0.58 mW) as well as sensitivities and resolutions for the out-of-plane and in-plane field of 12.98 V T^{-1}, 0.78 V T^{-1}, 135 nT $Hz^{-1/2}$, and 445 nT $Hz^{-1/2}$, respectively. Although, it needs vacuum (1 mbar) packaging and presents a residual motion induced by the electrostatic force, which causes an offset of the output voltage.

Wu et al. [25] designed a magnetometer with a square silicon plate (1000 × 1000 × 46 μm) and a planar induction coil (0.4 μm thick). It is fabricated using cavity-SOI process. It involves capacitive driving and electromagnetic induction to detect the external magnetic field. This silicon plate operates at resonance with a square-extensional (SE) vibration mode. The induction coil located on silicon plate has motion through magnetic field when the plate oscillates at resonance. The magnetometer has a sensitivity of 3 mV T^{-1} and a large output voltage offset (∼1.9 mV). A vacuum packaging is required to increase the magnetometer sensitivity.

Langfelder et al. [26] presented a magnetic field sensor formed by capacitive polysilicon plates with high aspect ratio that could have potential applications in inertial measurement units (IMUs). It has a compact structure with a sensitivity of 150 V T^{-1} at 250 μA of peak driving current. This sensor requires vacuum packaging (1 mbar) and has a non-linear electrical response.

3.3 Optical Sensing

Keplinger et al. [27, 28] designed two magnetometers with U-shaped silicon cantilevers (1100 × 100 × 10 μm) with an optical detection system (see Fig. 14). These magnetometers are appropriate to detect magnetic field from 10 mT up 50 T in electromagnetically noisy environments. They require an almost perfect vertical front side of the cantilevers. Temperature shifts can alter the fundamental resonant frequencies of the cantilevers, modifying the deflections and output signals of the magnetometers.

Wickenden et al. [29] developed a magnetometer formed by a polysilicon xylophone microbar (500 × 50 × 2 μm), as shown in Fig. 15. It converts the magnetic input signal into an oscillating motion of the xylophone microbar. This motion can be detected by an optical readout system based on a laser diode beam

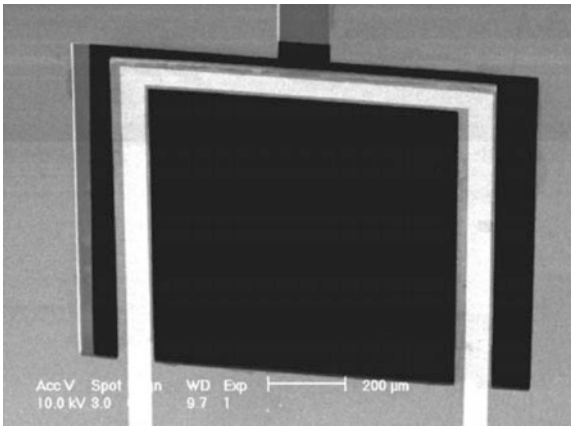

Fig. 14 SEM image of a magnetometer integrated by a resonant silicon structure with optical sensing [28]. The resonant-structure position is measured using an optical fiber. Reprinted with permission from Keplinger et al., Sens. Actuators A, 110, 112–118, 2004. Copyright © 2004, Elsevier B.V

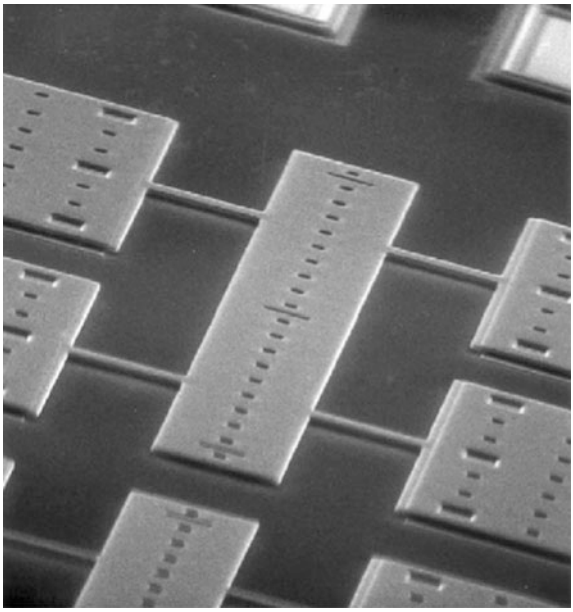

Fig. 15 SEM image of a magnetometer composed by a polysilicon xylophone bar resonator [29]. Reprinted with permission from Wickenden et al., Act. Astronaut., 52, 421–425, 2003. Copyright © 2003, Elsevier B.V

and a position sensitive detector. The magnetometer has a resonant frequency of 78.15 kHz, a quality factor close to 7000 at 4.7 Pa, ac current of 22 μA, a thermal noise of 100 pT A $Hz^{1/2}$, and a resolution close to nanoteslas. In addition, the microsensors with optical sensing have immunity to EMI. Although, it has a linear response up to 150 μT and its performance changes due to variations of pressure and temperature. Magnetometers with optical readout systems can reduce their electronic circuitries and weights.

Table 1 Main characteristics of several MEMS magnetometers

Magnetometer	Sensing technique	Resonant frequency (kHz)	Quality factor	Size (resonant structure) (μm × μm)	Sensitivity
Herrera-May et al. [20]	Piezoresistive	136.52	842	400 × 150	0.403 V T^{-1}
Herrera-May et al. [21]	Piezoresistive	22.99	96.6	700 × 400	1.94 V T^{-1}
Dominguez-Nicolas et al. [22]	Piezoresistive	14.38	93	700 × 600	4.0 V T^{-1}
Brugger and Paul [23]	Capacitive	2.20	2400	2000 × 2000	1.45 MHz T^{-1}
Li et al. [24]	Capacitive	46.96	10000	1000 × 2000	12.98 V T^{-1}
Wu et al. [25]	Capacitive	4329	3700	1000 × 1000	3×10^{-3} V T^{-1}
Langfelder et al. [26]	Capacitive	28.3	328	89 × 868	150 V T^{-1}
Keplinger et al. [27, 28]	Optical	5.0	200	1100 × 1000	*
Wickenden et al. [29]	Optical	78.15	7000	500 × 50	*

*Data not available in the literature

3.4 Comparisons

Generally, MEMS magnetometers have important advantages such as small size, lightweight, low power consumption, low cost, high sensitivity, wide dynamic range, and easy signal conditioning. Table 1 shows the main characteristics of several MEMS magnetometers, which operate with Lorentz force. They could be used for potential applications such as telecommunications, industrial, military, biomedical, and consumer electronic products.

4 Challenges and Future Applications

MEMS magnetometers have important characteristics for future commercial markets. However, these magnetometers present several challenges such as the decrease of their output response offset, noise, temperature and humidity dependence, as well as have high reliability. In addition, researches of the magnetometers reliability are needed to study their performance under different environment and operation conditions. Future magnetometers will require be integrated with others devices on a single chip, which will allow the develop of multifunctional sensors for

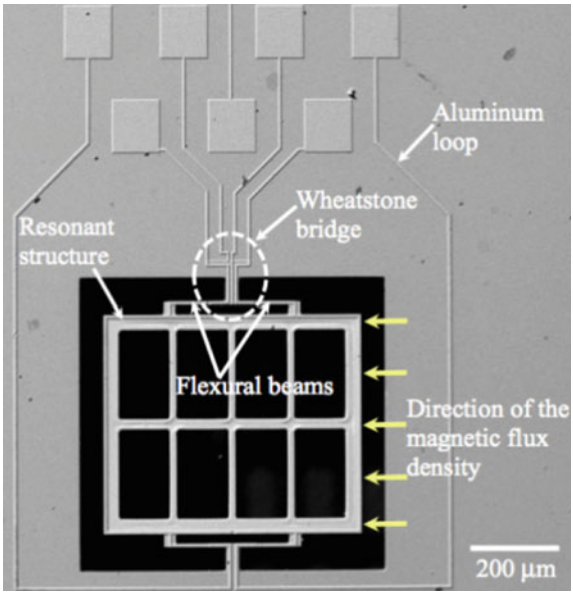

Fig. 16 SEM image of a MEMS magnetometer used for biomedical applications [30]. Reprinted with permission from Dominguez-Nicolás et al., Int. J. Med. Sci., 10, 1445–1450, 2013. Copyright © 2013, Ivyspring International Publisher

monitoring different chemical or physical signals such as gases, magnetic field, acceleration, pressure, and temperature.

A respiratory magnetogram had been developed using MEMS magnetometer (see Fig. 16), which can detect strong magnetic flux density during the respiratory activity of rats [30]. Figure 17a, b depicts the electromyogram and magnetogram of the thoracic cavity of a rat during its respiration [30]. These measurements could be useful in clinical diagnostics for monitoring the health of some organs of the thoracic cavity. Unhealthy organs could have variations of their magnetic flux density with respect to those obtained of healthy organs. For this biomedical application is necessary digital signal processing by virtual instrumentation of MEMS magnetometers [31].

MEMS magnetometers (see Figs. 18 and 19) could be employed to detect cracks and flaws of ferromagnetic materials through non-destructive testing (NDT) such as eddy current inspection and magnetic memory method (MMM) [32–35]. Eddy current technique requires the interaction between a magnetic field source and a ferromagnetic material, which induces eddy currents in the material. Small cracks of the material can be detected for monitoring changes of magnetic field generated by the eddy currents. MMM takes advantage of residual magnetic field of ferromagnetic materials, which can be generated during their fabrication processes or heat treatments. Cracks and geometrical defects of ferromagnetic materials cause variations of magnetic field that can be monitored through MEMS magnetometers.

Inertial measurement units (IMUs) can contain silicon magnetometers, accelerometers, and gyroscopes [26, 36]. These devices could be fabricated on a single chip to reduce the electronic noise and power consumption. IMUs have

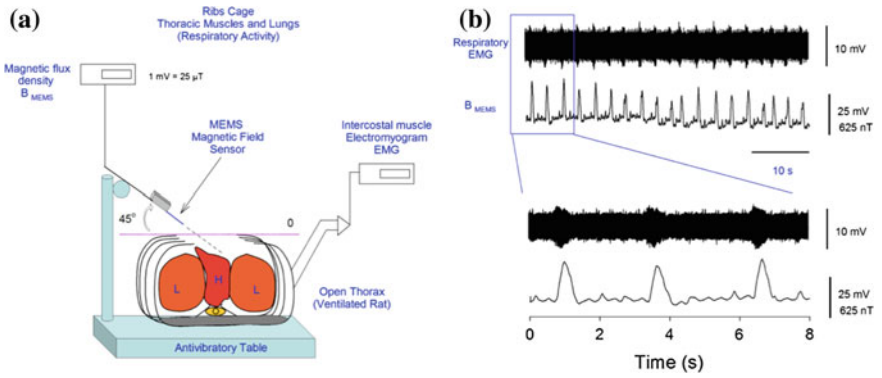

Fig. 17 **a** Diagram of experimental arrangement of a MEMS magnetometer used to measure the respiratory and cardiac activity of a rat. **b** Electromyogram of the thoracic muscles and magnetic flux density, which are detected during the respiratory activity of a rat [30]. Reprinted with permission from Dominguez-Nicolás et al., Int. J. Med. Sci., 10, 1445–1450, 2013. Copyright © 2013, Ivyspring International Publiser

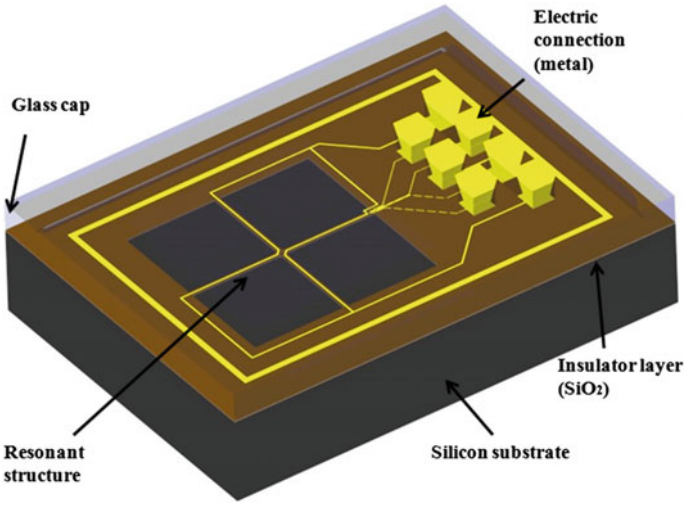

Fig. 18 Design a MEMS magnetometer with piezoresistive sensing with potential application for non-destructive testing (NDT) using the magnetic memory method [32]. Reprinted with permission from Acevedo-Mijangos et al., Microsyst. Technol., 19, 1897–1912, 2013. Copyright © 2013, Springer International Publishing AG

potential applications such as civil and military aviation, trains, space satellites, ships, consumer electronics, and unmanned operated vehicles [37–39]. Figure 20a–c shows a torsional MEMS magnetometer for monitoring in-plane magnetic field, which could be part of IMUs [36]. It operates with the Lorentz force and uses capacitive sensing. It has an area of 282 × 1095 μm, a packaged at nominal

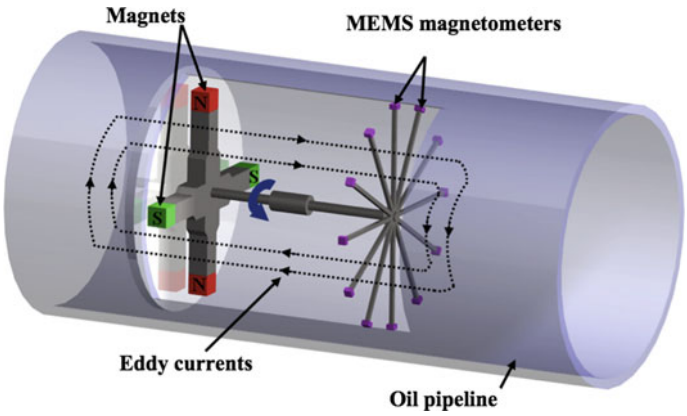

Fig. 19 Inspection system design for monitoring cracks in oil pipeline [34]. It requires eddy currents testing and MEMS magnetometers. Reprinted with permission from Herrera-May et al., Microsensors, Chap. 3, 65–84, 2011. Copyright © 2011, InTech

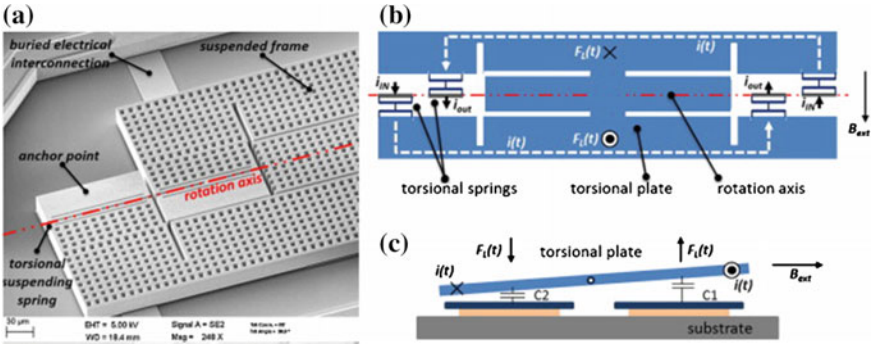

Fig. 20 SEM image of a torsional MEMS magnetometer for IMUs, fabricated using surface micromachining. **a** The magnetometer performance is schematized by the top view **b** and the cross-section **c** [36]. Reprinted with permission from Laghi et al., Sens. Actuat. A, 229, 218–226, 2015. Copyright © 2015, Elsevier B.V

pressure of 0.35 mbar, a resonant frequency of 19.95 kHz, a quality factor of 2500, and a sensitivity of 850 V T^{-1}.

Micro-, nano- or pico-satellites require low mass, small size and low power consumption magnetometers for their space missions. It can be overcome using magnetometers based on polysilicon-xylophone bars that operate at resonance with capacitive sensing [40, 41].

Electronic stability program (EPS) keeps the automotive dynamically stable in critical situations such as hard braking and slippery surfaces. EPS systems require data related with steering-wheel angle, yaw rate, lateral accelerations, and wheel speed. They could be measured through MEMS magnetometers, accelerometers,

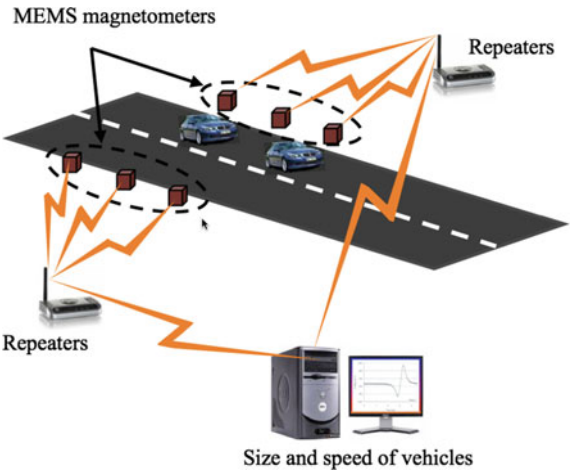

Fig. 21 Schematic diagram of a traffic detection system achieved with MEMS magnetometers [34]. Reprinted with permission from Herrera-May et al., Microsensors, Chap. 3, 65–84, 2011. Copyright © 2011, InTech

gyroscopes, and pressure devices. In addition, magnetometers could be applied in a traffic detection system to detect the speed and size of vehicles, as shown in Fig. 21. This system could be composed by two magnetometers (with a constant separation distance) located in parallel beside the road. Magnetometers will detect the change of the Earth's magnetic field caused by the vehicles motion that will be preceded to A/D converter and digital data processing system. The magnetic field shift will depend of the vehicles' speed and size, which will be detected by the magnetometers in different times (t_1 and t_2). Next, the vehicle speed will be calculated through the ratio of the magnetometers separation distance to the time difference $t_1 - t_2$. In addition, this system with an intelligent signal control could be used to decrease traffic congestion on roads.

5 Conclusions

MEMS technology has allowed the development of magnetometers composed by resonant silicon structures that exploit the Lorentz force. These MEMS magnetometers can be an important option with respect to conventional magnetometers due to their small size, low power consumption, wide dynamic range, high sensitivity and high resolution, and low cost by using batch fabrication. In addition, they could have future commercial markets, including biomedicine, telecommunications, aerospace, and automotive sector. Nevertheless, magnetometers reliability studies are needed to predict their performance under different environment and operation conditions. In addition, monolithic fabrication can be used to develop MEMS magnetometers with low electronic noise.

Acknowledgments This work was partially supported by Sandia National Laboratory's University Alliance Program, FORDECYT-CONACYT through grant 115976, and projects PRODEP "Estudio de Dispositivos Electrónicos y Electromecánicos con Potencial Aplicación en Fisiología y Optoelectrónica" and "Sistema Electrónico de Medición de Campo Magnético Residual de Estructuras Ferromagnéticas". The authors would like to thank Dr. Eduard Figueras of IMB-CNM (CSIC) for his collaboration into the fabrication of MEMS magnetometers and B.S. Fernando Bravo-Barrera of LAPEM for his assistance with the SEM images.

References

1. G.K. Ananthasuresh, K.J. Vinoy, S. Gopalakrishnan, K.N. Bhat, V.K. Aatre, *Micro and Smart Systems Technology and Modeling* (Wiley, Danvers, 2012)
2. S.D. Senturia, *Microsystem Design* (Kluwer Academic Publishers, New York, 2002)
3. A.L. Herrera-May, L.A. Aguilera-Cortés, P.J. García-Ramírez, E. Manjarrez, Resonant magnetic field sensor based on MEMS technology. Sensors **9**, 7785–7813 (2009)
4. O. Solgaard, A.A. Godil, R.T. Howe, L.P. Lee, Y.-A. Peter, H. Zappe, Optical MEMS: from micromirrors to complex systems. J. Microelectromech. Syst. **23**, 517–538 (2014)
5. D. Yamane, T. Konishi, T. Matsushima, K. Machida, H. Toshiyoshi, K. Masu, Design of sub-1 g microelectromechanical systems accelerometers. Appl. Phy. Lett. **104**, 074102Ç (2014)
6. Z. Deyhim, Z. Yousefi, H.B. Ghavifekr, E.N. Aghdam, A high sensitive and robust controllable MEMS gyroscope with inherently linear control force using a high performance 2-DOF oscillator. Microsyst. Technol. **21**, 227–237 (2015)
7. A.L. Herrera-May, J.A. Tapia, S.M. Domínguez-Nicolás, R. Juarez-Aguirre, E.A. Gutierrez-D, A. Flores, E. Figueras, E. Manjarrez, Improved detection of magnetic signals by a MEMS sensor using stochastic resonance. PLoS ONE **9**, e109534 (2014)
8. S. Kulwant, J. Robin, V. Soney, J. Akhtar, Fabrication of electron beam physical vapor deposited polysilicon piezoresistive MEMS pressure sensor. Sens. Actuators A **223**, 151–158 (2015)
9. Y. Liu, P. Song, J. Liu, D.J.H. Tng, R. Hu, H. Chen, Y. Hu, C.H. Tan, J. Wang, J. Liu, L. Ye, K.-T. Yong, An in-vivo evaluation of a MEMS drug delivery device using Kunming mice model. Biomed. Microdevices **17**, 6 (2015)
10. W. Zhenlu, S. Xuejin, C. Xiaoyang, Design, modeling, and characterization of a MEMS electrothermal microgripper. Microsyst. Technol. **21**, 2307–2314 (2015)
11. H. Tai-Ran, *MEMS & Microsystems. Design and Manufacture* (McGraw Hill, New York, 2002)
12. S. Sedky, *Post-processing Techniques for Integrated MEMS* (Artech House, Norwood, 2006)
13. A.L. Herrera-May, M. Lara-Castro, F. López-Huerta, P. Gkotsis, J.-P. Raskin, E. Figueras, A MEMS-based magnetic field sensor with simple resonant structure and linear electrical response. Microelectron. Eng. **142**, 12–21 (2015)
14. "MEMS Packaging," Yole Développement report. http://www.i-micronews.com/mems-sensors-report/product/mems-packaging.html
15. O. Tabata, T. Tsuchiya, MEMS and NEMS Simulation, in *MEMS: A Practical Guide to Design, Analysis, and Applications*, ed. by J.G. Korvink, O. Paul (William Andrew Inc, New York, 2006), pp. 53–186
16. F.R. Bloom, S. Bouwstra, M. Elwenspoek, J.H.J. Fluitman, Dependence of the quality factor of micromachined silicon beam resonators on pressure and geometry. J. Vac. Sci. Technol. B **10**, 19–26 (1992)
17. A.L. Herrera-May, L.A. Aguilera-Cortés, L. García-González, E. Figueras-Costa, Mechanical behavior of a novel resonant microstructure for magnetic applications considering the squeeze-film damping. Microsyst. Technol. **15**, 259–268 (2009)

18. R. Lifshit, M.L. Roukes, Thermoelastic damping in micro-and nanomechanical systems. Phys. Rev. B **61**, 5600–5609 (2000)
19. Z. Hao, A. Erbil, F. Ayazi, An analytical model for support loss in micromachined beam resonators with in-plane flexural vibrations. Sens. Actuators A **109**, 156–164 (2003)
20. A.L. Herrera-May, P.J. García-Ramírez, L.A. Aguilera-Cortés, J. Martínez-Castillo, A. Sauceda-Carvajal, L. García-González, E. Figueras-Costa, A resonant magnetic field microsensor with high quality factor at atmospheric pressure. J. Micromech. Microeng. **19**, 15016 (2009)
21. A.L. Herrera-May, P.J. García-Ramírez, L.A. Aguilera-Cortés, E. Figueras, J. Martínez-Castillo, E. Manjarrez, A. Sauceda, L. García- González, R. Juárez-Aguirre, Mechanical design and characterization of a resonant magnetic field microsensor with linear response and high resolution. Sens. Actuators A **165**, 299–409 (2011)
22. S.M. Dominguez-Nicolas, R. Juarez-Aguirre, P.J. Garcia-Ramirez, A.L. Herrera-May, Signal conditioning system with a 4–20 mA output for a resonant magnetic field sensor based on MEMS technology. IEEE Sens. J. **12**, 935–942 (2012)
23. S. Brugger, O. Paul, Field-concentrator-based resonant magnetic sensor with integrated planar coils. J. Microelectromech. Syst. **18**, 1432–1443 (2009)
24. M. Li, V.T. Rouf, M.J. Thompson, D.A. Horsley, Three-axis Lorentz-force magnetic sensor for electronic compass applications. J. Microelectromech. Syst. **21**, 1002–1010 (2012)
25. G. Wu, D. Xu, B. Xiong, D. Feng, Y. Wang, Resonant magnetic field sensor with capacitive driving and electromagnetic induction sensing. IEEE Electron Devices Lett. **34**, 459–461 (2013)
26. G. Langfelder, C. Buffa, A. Frangi, A. Tocchio, E. Lasalandra, A. Longoni, Z-axis magnetometers for MEMS inertial measurement units using an industrial process. IEEE Trans. Industr. Electron. **60**, 3983–3990 (2013)
27. F. Keplinger, S. Kvasnica, H. Hauser, R. Grössinger, Optical readouts of cantilever bending designed for high magnetic field application. IEEE Trans. Magn. **39**, 3304–3306 (2003)
28. F. Keplinger, S. Kvasnica, A. Jachimowicz, F. Kohl, J. Steurer, H. Hauser, Lorentz force based magnetic field sensor with optical readout. Sens. Actuators A **110**, 112–118 (2004)
29. D.K. Wickenden, J.L. Champion, R. Osiander, R.B. Givens, J.L. Lamb, J.A. Miragliotta, D.A. Oursler, T.J. Kistenmacher, Micromachined polysilicon resonating xylophone bar magnetometer. Acta Astronaut. **52**, 421–425 (2003)
30. S.M. Domínguez-Nicolás, R. Juárez-Aguirre, A.L. Herrera-May, P.J. García-Ramírez, E. Figueras, E. Gutierrez, J.A. Tapia, A. Trejo, E. Manjarrez, Respiratory magnetogram detected with a MEMS device. Int. J. Med. Sci. **10**, 1445–1450 (2013)
31. R. Juárez-Aguirre, S.M. Domínguez-Nicolás, E. Manjarrez, J.A. Tapia, E. Figueras, H. Vázquez-Leal, L.A. Aguilera-Cortés, A.L. Herrera-May, Digital signal processing by virtual instrumentation of a MEMS magnetic field sensor for biomedical applications. Sensors **13**, 15068–15084 (2013)
32. J. Acevedo-Mijangos, C. Soler-Balcázar, H. Vazquez-Leal, J. Martínez-Castillo, A.L. Herrera-May, Design and modeling of a novel microsensor to detect magnetic fields in two orthogonal directions. Microsyst. Technol. **19**, 1897–1912 (2013)
33. A. Dubov, A. Dubov, S. Kolokolnikov, Application of the metal magnetic memory method for detection of defects at the initial stage of their development for prevention of failures of power engineering welded steel structures and steam turbine parts. Weld World **58**, 225–236 (2014)
34. A.L. Herrera-May, L.A. Aguilera-Cortés, P.J. García-Ramírez, N.B. Mota-Carrillo, W.Y. Padrón-Hernández, E. Figueras, Development of Resonant Magnetic Field Microsensors: Challenges and Future Applications, in *Microsensors*, ed. by I. Minin (InTech, Croatia, 2011), pp. 65–84
35. M. Lara-Castro, A.L. Herrera-May, R. Juarez-Aguirre, F. López-Huerta, C.A. Ceron-Alvarez, I.E. Cortes-Mestizo, E.A. Morales-Gonzalez, H. Vazquez-Leal, S.M. Dominguez-Nicolas, Portable signal conditioning system of a MEMS magnetic field sensor for industrial applications. Microsyst. Technol. (2016). doi:10.1007/s00542-016-2816-4

36. G. Laghi, S. Dellea, A. Longoni, P. Minotti, A. Tocchio, S. Zerbini, G. Lagfelder, Torsional MEMS magnetometer operated off-resonance for in-plane magnetic field detection. Sens. Actuators A **229**, 218–226 (2015)
37. C.M.N. Brigante, N. Abbate, A. Basile, A.C. Faulisi, S. Sessa, Towards miniaturization of a MEMS-based wearable motion capture system. IEEE Trans. Industr. Electron. **58**, 3234–3241 (2011)
38. S.P. Won, F. Golnaraghi, W.W. Melek, A fastening tool tracking system using an IMUand a position sensor with Kalman filters and a fuzzy expert system. IEEE Trans. Industr. Electron. **56**, 1782–1792 (2009)
39. R.N. Dean, A. Luque, Applications of microelectromechanical systems in industrial processes and services. IEEE Trans. Industr. Electron. **56**, 913–925 (2009)
40. H. Lamy, V. Rochus, I. Niyonzima, P. Rochus, A xylophone bar magnetometer for micro/pico satellites. Acta Astronaut. **67**, 793–809 (2010)
41. S. Ranvier, V. Rochus, S. Druart, H. Lamy, P. Rochus, L.A. Francis, Detection methods for MEMS-Based xylophone bar magnetometer for pico satellites. J. Mech. Eng. Autom. **1**, 342–350 (2011)